measures of distance such as Euclidean are considered in Chapter 8.) Intuitively, the distance transform can be achieved by successive erosion and each pixel is labelled with the number of erosions before it disappeared. Accordingly, the pixels at the border of a shape will have a distance transform of unity, those adjacent inside will have a value of two, and so on. This is illustrated in Figure 6.14, where Figure 6.14(a) shows the analysed shape (a rectangle derived by, say, thresholding an image; the superimposed pixel values are arbitrary here as it is simply a binary image) and Figure 6.14(b) shows the distance transform, where the pixel values are the distance. Here, the central axis has a value of 3, as it takes that number of erosions to reach it from either side.

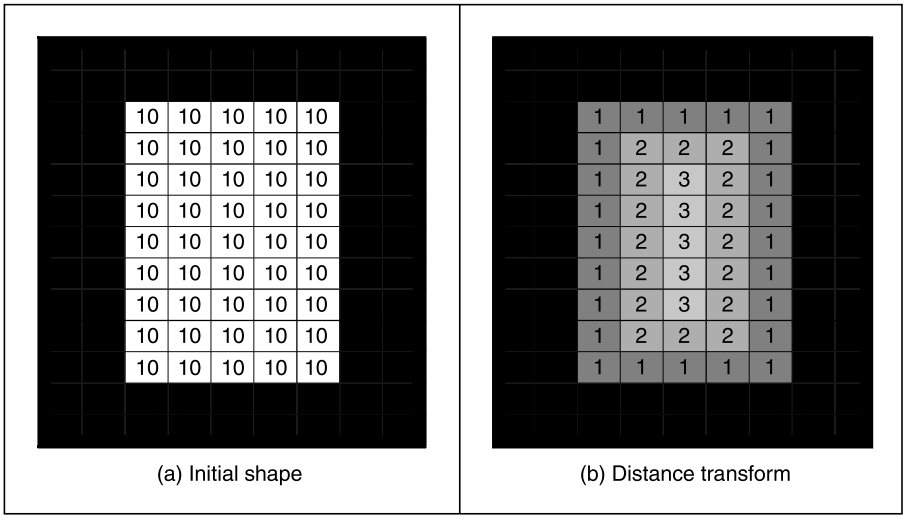

Figure 6.14 Illustrating distance transformation

The application to a rectangle at higher resolution is shown in Figure 6.15(a) and (b). Here, we can see that the central axis is quite clear and includes parts that reach towards the corners; and the central axis can be detected (Niblack et al., 1992) from the transform data. The application to a more irregular shape is shown applied to that of a card suit in Figure 6.15(c) and (d).

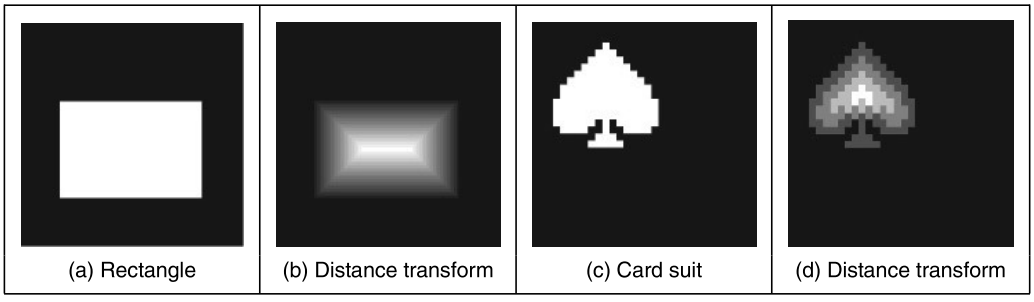

Figure 6.15 Applying the distance transformation

The natural difficulty is the effect of noise. This can change the result, as shown in Figure 6.16. This can certainly be ameliorated by using the earlier morphological operators (Section 3.6) to clean the image, but this can obscure the shape when the noise is severe. The major point is that this noise shows that the effect of a small change in the object can be quite severe on the resulting distance transform. As such, it has little tolerance of occlusion or change to its perimeter.

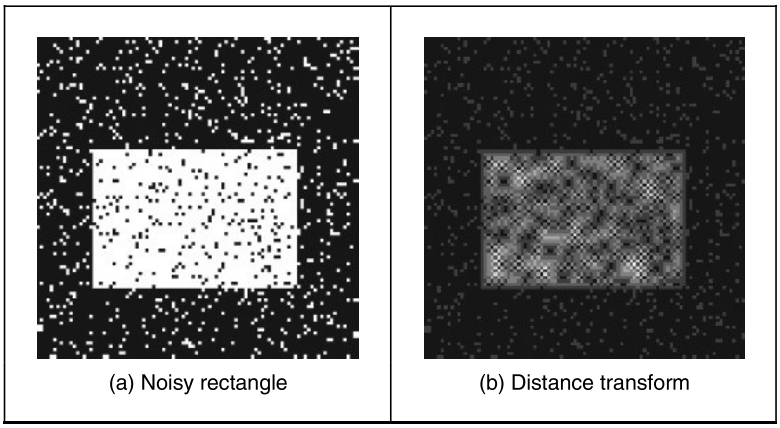

Figure 6.16 Distance transformation on noisy images

The natural extension from distance transforms is to the *medial axis transform* (Blum, 1967), which determines the skeleton that consists of the locus of all the centres of maximum disks in the analysed region/shape. This has found use in feature extraction and description, so approaches have considered improvement in *speed* (Lee, 1982). One more recent study (Katz and Pizer, 2003) noted the practically difficulty experienced in *noisy* imagery: 'It is well documented how a tiny change to an object's boundary can cause a large change in its Medial Axis Transform'. To handle this, and hierarchical shape decomposition, the new approach 'provides a natural parts-hierarchy while eliminating instabilities due to small boundary changes'. An alternative is to seek an approach that is designed explicitly to handle noise, say by averaging, and we shall consider this type of approach next.

6.4.2 Symmetry

The *discrete symmetry operator* (Reisfeld et al., 1995) uses a totally different basis to find shapes, is intuitively very appealing and has links with human perception. Rather than rely on finding the border of a shape, or its shape, it locates features according to their *symmetrical properties*. The operator essentially forms an *accumulator* of points that are measures of symmetry between image points. Pairs of image points are attributed symmetry values that are derived from a *distance* weighting function, a *phase* weighting function and the *edge* magnitude at each of the pair of points. The distance weighting function controls the scope of the function, to control whether points that are more distant contribute in a similar manner to those that are close together. The phase weighting function shows when edge vectors at the pair of points point to each other. The symmetry accumulation is at the centre of each pair of points. In this way, the

accumulator measures the degree of symmetry between image points, controlled by the edge strength. The distance weighting function D is

$$D(i, j, \sigma) = \frac{1}{\sqrt{2\pi\sigma}} e^{-\frac{|\mathbf{P}_i - \mathbf{P}_j|}{2\sigma}} \tag{6.59}$$

where i and j are the indices to two image points $\mathbf{P}_i$ and $\mathbf{P}_j$ and the deviation σ controls the scope of the function, by scaling the contribution of the distance between the points in the exponential function. A small value for the deviation σ implies local operation and detection of local symmetry. Larger values of σ imply that points that are further apart contribute to the accumulation process, as well as ones that are close together. In, say, application to the image of a face, large and small values of σ will aim for the whole face or the eyes, respectively.

The effect of the value of σ on the scalar distance weighting function expressed as Equation 6.60 is illustrated in Figure 6.17.

$$Di(j, \sigma) = \frac{1}{\sqrt{2\pi\sigma}} e^{\frac{j}{\sqrt{2\sigma}}} \tag{6.60}$$

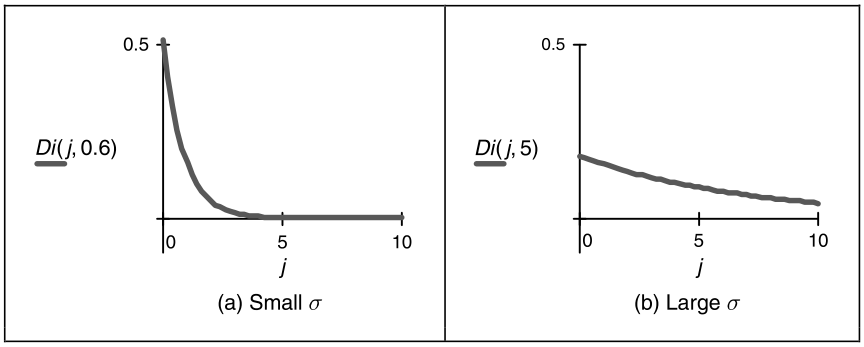

Figure 6.17 Effect of σ on distance weighting

Figure 6.17(a)shows the effect of a small value for the deviation, $\sigma = 0.6$, and shows that the weighting is greatest for closely spaced points and drops rapidly for points with larger spacing. Larger values of σ imply that the distance weight drops less rapidly for points that are more widely spaced, as in Figure 6.17(b) where $\sigma = 5$, allowing points that are spaced further apart to contribute to the measured symmetry. The phase weighting function P is

$$P(i, j) = (1 - \cos(\theta_i + \theta_j - 2\alpha_{ij})) \times (1 - \cos(\theta_i - \theta_j)) \tag{6.61}$$

where θ is the edge direction at the two points and α_{ij} measures the direction of a line joining the two points:

$$\alpha_{ij} = \tan^{-1}\left(\frac{y(\mathbf{P}_j) - y(\mathbf{P}_i)}{x(\mathbf{P}_j) - x(\mathbf{P}_i)}\right) \tag{6.62}$$

where $x(\mathbf{P}_i)$ and $y(\mathbf{P}_i)$ are the x and y coordinates of the point $\mathbf{P}_i$, respectively. This function is minimum when the edge direction at two points is in the same direction ($\theta_j = \theta_i$), and is a maximum when the edge direction is away from each other ($\theta_i = \theta_j + \pi$), along the line joining the two points, ($\theta_j = \alpha_{ij}$).

The effect of relative edge direction on phase weighting is illustrated in Figure 6.18, where Figure 6.18(a) concerns two edge points that point towards each other and describes the effect on the phase weighting function by varying α_{ij}. This shows how the phase weight is maximum when the edge direction at the two points is along the line joining them, in this case when $\alpha_{ij} = 0$ and $\theta_i = 0$. Figure 6.18(b) concerns one point with edge direction along the line joining two points, where the edge direction at the second point is varied. The phase weighting function is maximum when the edge direction at each point is towards that of the other, in this case when $|\theta_j| = \pi$.

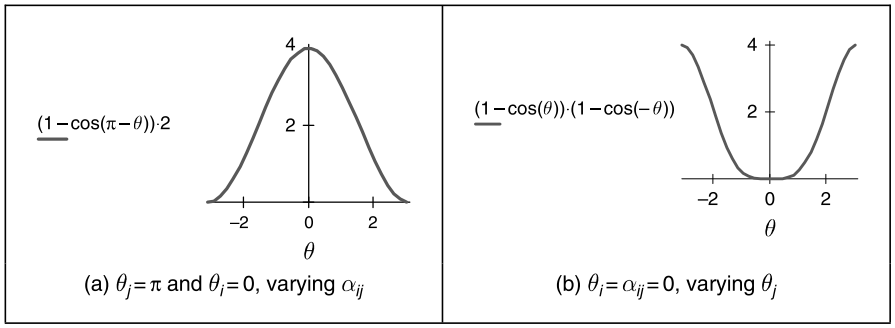

Figure 6.18 Effect of relative edge direction on phase weighting

The symmetry relation between two points is then defined as

$$C(i, j, \sigma) = D(i, j, \sigma) \times P(i, j) \times E(i) \times E(j) \tag{6.63}$$

where E is the edge magnitude expressed in logarithmic form as

$$E(i) = \log(1 + M(i)) \tag{6.64}$$

where M is the edge magnitude derived by application of an edge detection operator. The symmetry contribution of two points is accumulated at the midpoint of the line joining the two points. The total symmetry $S_{\mathbf{P}_m}$ at point $\mathbf{P}_m$ is the sum of the measured symmetry for all pairs of points which have their midpoint at $\mathbf{P}_m$, i.e. those points $\Gamma(\mathbf{P}_m)$ given by

$$\Gamma(\mathbf{P}_m) = \left[(i, j) \left| \frac{\mathbf{P}_i + \mathbf{P}_j}{2} = \mathbf{P}_m \wedge i \neq j \right. \right] \tag{6.65}$$

and the accumulated symmetry is then

$$S_{\mathbf{P}_m}(\sigma) = \sum_{i,j \in \Gamma(\mathbf{P}_m)} C(i, j, \sigma) \tag{6.66}$$

The result of applying the symmetry operator to two images is shown in Figure 6.19, for small and large values of σ. Figure 6.19(a) and (d) show the image of a rectangle and the image of the club, respectively, to which the symmetry operator was applied, and Figure 6.19(b) and (e) for the symmetry operator with a *low* value for the deviation parameter, showing detection of areas with high localized symmetry. Figure 6.19(c) and (f) are for a *large* value of the deviation parameter which detects overall symmetry and places a peak near the centre of the target shape. In Figure 6.19(b) and (e) the symmetry operator acts as a corner detector where the edge direction is discontinuous. (Note that this rectangle is one of the synthetic images we can use

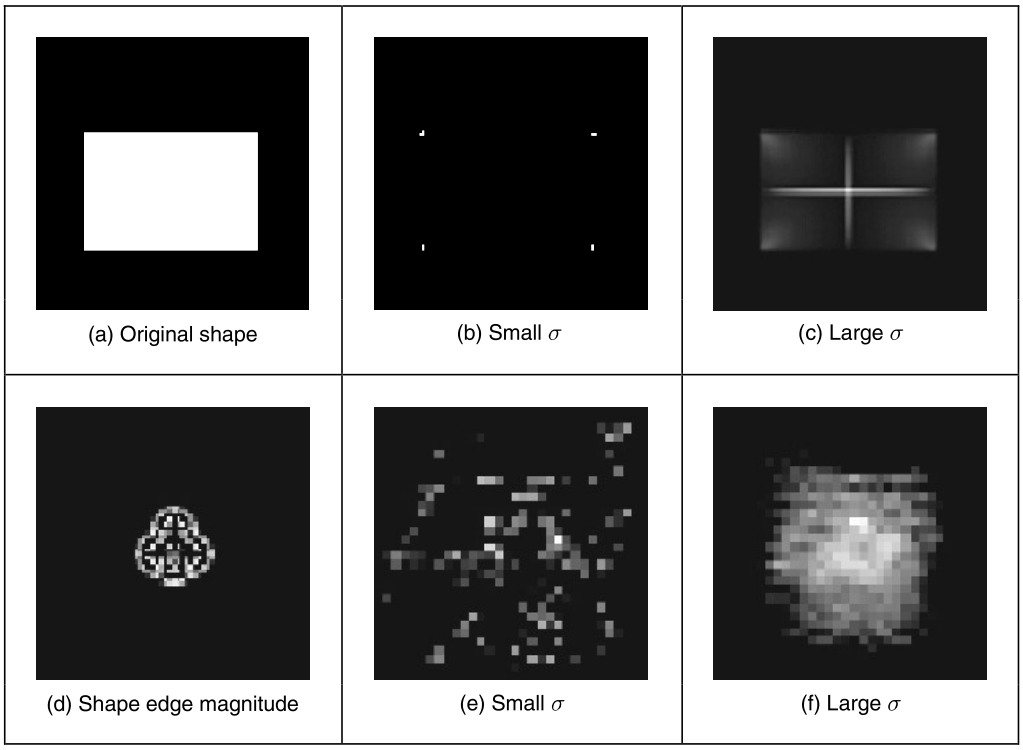

Figure 6.19 Applying the symmetry operator for feature extraction

to test techniques, since we can understand its output easily. We also tested the operator on the image of a circle; since the circle is completely symmetrical, its symmetry plot is a single point, at the centre of the circle.) In Figure 6.19(e), the discrete symmetry operator provides a peak close to the position of the accumulator space peak in the GHT. Note that if the reference point specified in the GHT is the centre of symmetry, the results of the discrete symmetry operator and the GHT would be the same for large values of deviation.

This is a discrete operator; a *continuous symmetry operator* has been developed (Zabrodsky et al., 1995), and a later clarification (Kanatani, 1997) aimed to address potential practical difficulty associated with *hierarchy* of symmetry (namely that symmetrical shapes have subsets of regions, also with symmetry). There has also been a number of sophisticated approaches to detection of *skewed symmetry* (Gross and Boult, 1994; Cham and Cipolla, 1995), with later extension to detection in *orthographic projection* (Vangool et al., 1995). Another generalization addresses the problem of *scale* (Reisfeld, 1996) and extracts points of symmetry, together with scale. A *focusing* ability has been added to the discrete symmetry operator by reformulating the distance weighting function (Parsons and Nixon, 1999) and we able were to deploy this when using symmetry to in an approach which recognizes people by their gait (the way they walk) (Hayfron-Acquah et al., 2003). Why symmetry was chosen for this task is illustrated in Figure 6.20: this shows the main axes of symmetry of the walking subject (Figure 6.20b), that exist within the body, largely defining the skeleton. There is another axis of symmetry, between the legs. When the symmetry operator is applied to a sequence of images, this axis grows and retracts. By agglomerating the sequence and describing it by a (low-pass filtered)